

INFORMATION TO USERS

This manuscript has been reproduced from the microfilm master. UMI films the text directly from the original or copy submitted. Thus, some thesis and dissertation copies are in typewriter face, while others may be from any type of computer printer.

The quality of this reproduction is dependent upon the quality of the copy submitted. Broken or indistinct print, colored or poor quality illustrations and photographs, print bleedthrough, substandard margins, and improper alignment can adversely affect reproduction.

In the unlikely event that the author did not send UMI a complete manuscript and there are missing pages, these will be noted. Also, if unauthorized copyright material had to be removed, a note will indicate the deletion.

Oversize materials (e.g., maps, drawings, charts) are reproduced by sectioning the original, beginning at the upper left-hand corner and continuing from left to right in equal sections with small overlaps. Each original is also photographed in one exposure and is included in reduced form at the back of the book.

Photographs included in the original manuscript have been reproduced xerographically in this copy. Higher quality 6" x 9" black and white photographic prints are available for any photographs or illustrations appearing in this copy for an additional charge. Contact UMI directly to order.

UMI

A Bell & Howell Information Company
300 North Zeeb Road, Ann Arbor MI 48106-1346 USA
313/761-4700 800/521-0600

PREVIEW

**MICROCLIMATE INSIDE AIR TEMPERATURE
RADIATION SHIELDS**

by

Xiaomao Lin

A DISSERTATION

Presented to the Faculty of

The Graduate College in the University of Nebraska

In Partial Fulfillment of Requirements

For the Degree of Doctor of Philosophy

Major: Agronomy

Under the Supervision of Professor Kenneth G. Hubbard

Lincoln, Nebraska

May, 1999

UMI Number: 9929212

Copyright 1999 by
Lin, Xiaomao

All rights reserved.

UMI Microform 9929212
Copyright 1999, by UMI Company. All rights reserved.

This microform edition is protected against unauthorized
copying under Title 17, United States Code.

UMI

300 North Zeeb Road
Ann Arbor, MI 48103

DISSERTATION TITLE

MICROCLIMATE INSIDE AIR TEMPERATURE
RADIATION SHIELDS

BY

XIAOMAO LIN

SUPERVISORY COMMITTEE:

APPROVED

DATE

Kenneth G. Hubbard
Signature

April 27, 1999

Dr. Kenneth G. Hubbard
Typed name

Elizabeth A. Walter-Shea
Signature

April 27, 1999

Dr. Elizabeth Walter-Shea
Typed name

James R. Brandle
Signature

4/27/99

Dr. James R. Brandle
Typed name

George E. Meyer
Signature

April 27, 1999

Dr. George E. Meyer
Typed name



GRADUATE COLLEGE
UNIVERSITY OF NEBRASKA

MICROCLIMATE INSIDE AIR TEMPERATURE RADIATION SHIELDS

Xiaomao Lin, Ph. D.

University of Nebraska, 1999

Advisor: Kenneth G. Hubbard

With the replacement of the Cotton Region Shelter (CRS), new air temperature observing systems such as the Automated Surface Observing System (ASOS), Maximum-Minimum Temperature System (MMTS), and the Gill shield temperature system were introduced. All of these systems house the air temperature sensor in radiation shields to prevent radiation loading on the sensors; a side-effect is that the air temperature entering a shield is modified by the interior solar radiation, infrared radiation, air speed, and heat conduction to or from the sensor so that the shield forms its own interior microclimate. The objectives of this study are to: 1. Theoretically investigate air temperature errors inside radiation shields. 2. Experimentally determine the air flow characteristics inside the shields. 3. Develop a physical model to understand the microclimate inside the shields including the interior solar radiation, infrared radiation, and air speed effects on the air (sensor) temperature under day and night conditions. 4. Experimentally estimate the effect of underlying ground surface coverings on the shield's interior solar radiation.

Theoretical investigation, field experiments, and the energy balance modeling of

temperature sensors were methodologies in this study. Parabolic curves described the fraction of solar radiation entering shields during the day light hours. This fraction increased as the ground solar reflectivity increased, except for the ASOS, as a function of time of day. The rank of solar radiation shielding effectiveness was $ASOS > CRS > MMTS > Gill$. The ASOS dew point sensor extracted heat from the mirror surface and heated or cooled the shield. The rank for the magnitude of unbalanced infrared radiation was $ASOS > CRS > MMTS > Gill$. Linear equations provided a reliable air speed estimation inside the shields based on the ambient wind speed. The air flow efficiency of shields (exception of ASOS) ranked as $MMTS > CRS > Gill$ when the ambient wind speed was below 1 m s^{-1} and ranked as $Gill > MMTS > CRS$ when the ambient wind speed was more than 2 m s^{-1} . For all radiation shields, the air temperature corrected for shield effects was in good agreement between shields while the uncorrected "normal operating" temperatures were more variable from shield to shield.

ACKNOWLEDGMENTS

I express sincere appreciation and gratitude to Dr. Kenneth G. Hubbard, my advisor, for his guidance, patience and encouragement throughout my graduate education. I wish to thank Drs. Elizabeth A. Walter-Shea, James R. Brandle, and George E. Meyer for serving on the supervisory committee and providing helpful guidance and critical reviews.

I express special gratitude to Drs. Blaine L. Blad, Shashi B. Verma, and Albert Weiss for introducing me to Dr. Kenneth G. Hubbard as a graduate student so that I could pursue the higher education in a new country. I also thank Karl Blauvelt, Mark Mesarch, and James Hines for their technical assistance and suggestions during my study. I thank Dr. Kevin D. Cole in the Department of Mechanical Engineering with whom I consulted several times concerning radiation heat transfer.

A special thanks goes to the National Weather Service (NWS) for providing me a three-year fellowship award through UCAR to support my study at UNL. I also thank Vickie L. Nadolski (NWS) for the loan of two ASOS Hygrothermometers and Tom Blackburn (NWS) for the loan of two MMTS shields during this study.

My thanks also go to the other staff members in the SNRS Climate and Bio-Atmospheric Sciences Group for their valuable assistance, and to all my fellow graduate colleagues, but especially to Meng Xu, Qingwu Xue, Georgiy G. Burba, and Andy Suyker for their valuable help and humor.

Finally, I dedicate this work to my family. I am grateful to my wife Ruiju Yang for her love and support over the years. Thank you.

TABLE OF CONTENTS

	Page
ABSTRACT.....	i
ACKNOWLEDGMENTS	iii
CHAPTER 1. INTRODUCTION	1
CHAPTER 2. INVESTIGATION OF RADIATIVE ERROR INSIDE AIR TEMPERATURE RADIATION SHIELDS	6
2.1 Introduction	6
2.2 Materials and Methods	12
2.3 Results	23
2.4 Conclusions and Discussion	28
2.5 Recommendations	31
CHAPTER 3. AIR FLOW CHARACTERISTICS OF TEMPERATURE RADIATION SHIELDS	58
3.1 Introduction	58
3.2 Materials and Methods	61
3.3 Results	65
3.4 Conclusions and Discussion	69
3.5 Recommendations	73
CHAPTER 4. MODELING THE MICROCLIMATE INSIDE AIR TEMPERATURE RADIATION SHIELDS.....	86
4.1 Introduction	86
4.2 Materials and Methods	91
4.3 Results	102
4.4 Conclusions and Discussion	110
4.5 Recommendations	113
CHAPTER 5. EFFECT OF GROUND SURFACE CHARACTERISTICS ON AIR TEMPERATURE SHIELD PERFORMANCE	134
5.1 Introduction	134
5.2 Materials and Methods	135
5.3 Results	140

5.4 Conclusions and Discussion	143
5.5 Recommendations	144
CHAPTER 6. SUMMARY AND CONCLUSIONS	156
REFERENCES	160
APPENDIX	
A. The Effect of Choice of Materials on Shield Performance	170
B. Determination of Infrared Emissivity	186

PREVIEW

List of Figures

	Page
Figure 1 . 1 Air temperature radiation shields: the standard NWS Cotton Region Shield (CRS); Gill; the Maximum-Minimum Temperature System (MMTS); and the Hygrothermometer of the Automated Surface Observing System (ASOS)	5
Figure 2 . 1 Two types of reflective surfaces	32
Figure 2 . 2 Sketch showing area elements used in deriving radiation configuration factor	33
Figure 2 . 3 Sketch of the MMTS-sized radiation shield and temperature sensor	34
Figure 2 . 4 Cross section of Figure 2 . 3 with surface designations. All surface are diffuse reflecting surfaces	35
Figure 2 . 5 Complete analogous radiation network for the radiation shield and air temperature sensor in Figure 2 . 3	36
Figure 2 . 6 Convective heat-transfer coefficient (H) estimation for a spherical sensor (4mm in diameter) inside the shield	37
Figure 2 . 7 Installation of radiation shields and datalogger for solar radiation measurements inside the radiation shields	38
Figure 2 . 8 Sketch of ASOS temperature measurements system showing location of LI-200S inside the shield	39
Figure 2 . 9 Cross-section of MMTS shield showing location of LI-200S inside the shield	40
Figure 2 . 10 Cross-section of Gill shield showing location of LI-200S inside the shield	41
Figure 2 . 11 Sketch of Cotton Region Shelter (CRS) showing location of LI-200S inside the shield	42
Figure 2 . 12 Incoming global solar radiation (IGSR) for the incoming solar radiation measurements inside the shields, 1998. A. DOY 183. B. DOY 184. C. DOY 185. D. DOY 179. E. DOY 181. F. DOY 182.	43

Figure 2 . 13	Average ISRR% for six-height average inside the ASOS, MMTS, Gill, and CRS at DOY183, 184, 185, 179, 181, and DOY182, 1998. A. MMTS, Gill, and CRS measurements. B. ASOS measurements	44
Figure 2 . 14	ISRR% at the normal operating height for sensors inside the ASOS, MMTS, Gill, and CRS. A. MMTS and Gill are at DOY181, 1998; CRS is at DOY184, 1998. B. ASOS is at DOY184, 1998	45
Figure 2 . 15	Profiles of daily ISRR% for a day inside the shields	46
Figure 2 . 16	Incoming global solar radiation (IGSR) for the days when outgoing solar radiation measurements were taken inside the shields in 1998. A. DOY208. B. DOY230. A. DOY220. D. DOY229	47
Figure 2 . 17	A. Average OSRR% inside the ASOS, MMTS, Gill, and CRS at DOY229, 220, 230, and DOY208 in 1988, respectively. B. OSRR% at the normal operating height for sensors inside the ASOS, MMTS, Gill, and CRS at DOY208, 229, 220, and DOY208 in 1998, respectively	48
Figure 2 . 18	Profiles of daily OSRR% for a day inside the shields	49
Figure 2 . 19	Average TSRR% and profiles of daily TSRR% inside the shields A. Average TSRR%. B. Profiles of daily TSRR%.	50
Figure 2 . 20	Simulated air temperature, incoming global solar radiation (IGSR), and solar radiation loading inside the shield. A. Air temperature. B. IGSR. C. Solar radiation loading inside the shield	51
Figure 2 . 21	Simulated daytime air temperature error caused by the convective heat coefficient (H) and sensor emissivity. A. Sensor emissivity is 0.9. B. Sensor emissivity is 0.5. C. Sensor emissivity is 0.05	52
Figure 2 . 22	A. Simulated daytime temperature error under the different sensor emissivity at the solar time 10:00. B. Simulated daytime temperature error for the different inner	

	surface temperatures of shield and emissivity (both inner surfaces and sensor surface) = 0.9	53
Figure 2 . 23	Simulated nighttime temperature error under the different sensor emissivity at solar time 0:00. A. 1°C difference between the air and shield inner surface temperatures. B. 3°C difference between the air and shield inner surface temperatures.	54
Figure 2 . 24	Simulated nighttime temperature error for the different inner surface temperature of shield and emissivity (both inner surfaces and sensor surface) = 0.9	55
Figure 3 . 1	Detail of air flow turntable construction	74
Figure 3 . 2	Cross-section of the MMTS shield on the turntable. Omni-directional air velocity transducer TSI Model 8475 was as shown along the center line	75
Figure 3 . 3	Cross-section of the Gill shield on the turntable. Omni-directional air velocity transducer TSI Model 8475 was as shown along the center line	76
Figure 3 . 4	Air speed comparison between the TSI measurements and calculation from the Equation (3.2). The TSI sensor height during the measurements is 835 mm above the ground surface	77
Figure 3 . 5	Air flow profiles for nominal air (turntable) speed or 'turntable air' speed	78
Figure 3 . 6	A. Air flow speed profiles inside the MMTS on the turntable. B. Air flow efficiency profiles inside the MMTS on the turntable	79
Figure 3 . 7	A. Air flow speed profiles inside the Gill on the turntable. B. Air flow efficiency profiles inside the Gill on the turntable	80
Figure 3 . 8	A. Air flow speed at the normal operating sensor height inside the MMTS on the turntable. B. Air flow efficiency at the normal operating sensor height inside the MMTS on the turntable	81
Figure 3 . 9	A. Air flow speed at the normal operating sensor height inside the Gill on the turntable. B. Air flow efficiency at the normal operating sensor height inside the Gill on the turntable	82

Figure 3 . 10	Air speed at the normal operating sensor height inside the shields under the field condition. A. Inside the MMTS (n=3200); B. Inside the Gill (n=4058); C. Inside the CRS (n=5952).	83
Figure 3 . 11	Air flow efficiency at the normal operating sensor height inside the shields under the field condition. A. Inside the MMTS; B. Inside the Gill; C. Inside the CRS	84
Figure 4 . 1	Close-up of the prototype EBTC exposed without radiation shield. Exposed spherical painted thermocouples are 5.8 mm in diameter	115
Figure 4 . 2	Convective heat-transfer coefficient (H) estimation for EBTC sensor.	116
Figure 4 . 3	From the left, pairs of ASOS and MMTS shields, a CRS, a pair of Gill shields and Met-One wind speed and direction sensors, and an A-frame for auxiliary measurements. The surface is snow covered	117
Figure 4 . 4	White EBTC sensor's energy partition inside the CRS, DOY70, 1998. A. During the daytime. B. During the nighttime	118
Figure 4 . 5	A. Incoming global solar radiation (IGSR), DOY 227, 1997. B. Incoming global solar radiation (IGSR), DOY 70, 1998. C. Incoming global solar radiation (IGSR), DOY 71, 1998	119
Figure 4 . 6	NP air temperatures and EBTC modeling air temperatures inside the shields, DOY227, 1997. A. NP air temperatures inside the shields. B. EBTC modeling air temperatures inside the shields	120
Figure 4 . 7	EBTC solar radiation inside shields, DOY227, 1997. A. Inside the ASOS. B. Inside the MMTS. C. Inside the Gill. D. Inside the CRS	121
Figure 4 . 8	Temperature errors and ambient wind speed on DOY227, 1997. A. Temperature error inside the ASOS. B. Temperature error inside the MMTS. C. Temperature error inside the Gill and CRS. D. Ambient wind speed	122

Figure 4 . 9	NP air temperatures and EBTC modeling air temperatures inside the shields, DOY69 to DOY71, 1998. A. NP temperatures inside the shields. B. EBTC modeling temperatures inside the shields	123
Figure 4 . 10	EBTC solar radiation (SR) inside shields under snow covering surface. A. On DOY70, 1998. B. On DOY71, 1998	124
Figure 4 . 11	Temperature errors and ambient wind speed on DOY69 to 71, 1998. A. Temperature error inside the ASOS. B. Temperature error inside the MMTS. C. Temperature error inside the Gill and CRS. D. Ambient wind speed	125
Figure 4 . 12	A. Average IST for all the shields, DOY 227, 1997. B. The IST for the ASOS, DOY227, 1997	126
Figure 4 . 13	A. Average IST for the all shields, DOY69 to 71, 1998. B. The IST for the ASOS, DOY69 to 71, 1998	127
Figure 4 . 14	A. Average IST for all the shields in the consecutive two days, DOY 220 to DOY222, 1997. B. The IST for the ASOS in the consecutive two days, DOY220 to DOY222, 1997	128
Figure 4 . 15	NP air temperature errors, IGSR is above 800 W m^{-2} . A. For the ASOS NP air temperature system. B. For the MMTS NP air temperature system with CR10 datalogger. C. For the Gill NP air temperature with HMP35C sensor. D. For the CRS NP air temperature with HMP35C sensor	129
Figure 4 . 16	NP air temperature errors during the early morning from 3:00 to 4:30. A. For the ASOS NP air temperature system. B. For the MMTS NP air temperature system with CR10 datalogger. C. For the Gill NP air temperature with HMP35C sensor. D. For the CRS NP air temperature with HMP35C sensor	130
Figure 5 . 1	Comparison between the PSP and LI-200S inside the CRS and measurement of spectral reflectivity of the radiation shield surfaces. A. IGSR on DOY 285, 1998. B. IGSR on DOY 286, 1998.	

	B. Simulated solar radiation and infrared radiation received by an MMTS-sized cylindrically shaped shield under a typical cloudless day (in summer or fall)	180
Figure A . 3	Estimation of convection heat coefficient for the MMTS-sized cylindrically shield	181
Figure A . 4	Simulated temperature difference between the shield surface temperature and the air temperature for typical daytime conditions with a solar elevation (β) of 90° and varying convective heat coefficient conditions. A) $H = 5 \text{ W m}^{-2} \text{ K}^{-1}$, B) $H = 20 \text{ W m}^{-2} \text{ K}^{-1}$ C) $H = 40 \text{ W m}^{-2} \text{ K}^{-1}$, and D) $H = 60 \text{ W m}^{-2} \text{ K}^{-1}$	182
Figure A . 5	Simulated temperature difference between the shield surface temperature and the air temperature for typical daytime conditions with a solar elevation (β) of 45° and varying convective heat coefficient conditions. A) $H = 5 \text{ W m}^{-2} \text{ K}^{-1}$, B) $H = 20 \text{ W m}^{-2} \text{ K}^{-1}$ C) $H = 40 \text{ W m}^{-2} \text{ K}^{-1}$, and D) $H = 60 \text{ W m}^{-2} \text{ K}^{-1}$	183
Figure A . 6	Simulated temperature difference between the shield surface temperature and the air temperature for typical nighttime conditions with an air temperature of 25°C and varying convective heat coefficient conditions. A) $H = 5 \text{ W m}^{-2} \text{ K}^{-1}$, B) $H = 20 \text{ W m}^{-2} \text{ K}^{-1}$ C) $H = 40 \text{ W m}^{-2} \text{ K}^{-1}$, and D) $H = 60 \text{ W m}^{-2} \text{ K}^{-1}$	184
Figure B . 1	Schematic diagram of emissivity box.	190

PRE

List of Tables

	Page
Table 2 . 1	Geometrical dimensions of CRS, Gill, MMTS, and ASOS shields 56
Table 2 . 2	Summaries of known parameters in the Equation (2.8) to Equation (2.11) 57
Table 3 . 1	Summary of air flow efficiency of the radiation shields 85
Table 4 . 1	Solar absorptivity and infrared emissivity of the thermocouple coatings 131
Table 4 . 2	Temperature sensor's accuracy, resolution, and range 132
Table 4 . 3	EBTC modeling summaries of radiation heating or cooling effects on air temperature 133
Table 5 . 1	Experimental days, ground surface cover, and corresponding measurements for case studies 155
Table A . 1	Values of sensitivity analysis variables 185

PREVIEW

CHAPTER 1

INTRODUCTION

How can we find the true temperature signal of global warming? Despite the litany of problems, the instrumented climate record can tell us a great deal about the spatial distribution and secular trends in temperature over many areas of the world (Karl et al., 1989). The magnitude of changes in global mean temperature is one of the cornerstones of the greenhouse warming issue, however, the temperature sensor related biases found by Quayle et al. (1991) are of the same magnitude as the recorded change in global and United States mean temperatures since the turn of the century. Additional challenges in using the historical climate record are issues of calibration, observing practices, urbanization, station changes, data representativeness, data access, and areal coverage (Karl et al., 1986; 1987; 1988; 1989; 1993; Karl and Quayle, 1988; Karl and Jones, 1989). Inhomogeneities in surface weather records can and have produced a number of serious biases in the climate records. Researchers have focused on identifying and removing these biases that result from the above climate monitoring issues.

Changes in station location, instruments, instrument shelters, and the height of the instruments above the ground have lead to biases of 1 °C or more at many stations (Karl et al., 1987). Because of inadequate station meta-data and insufficient side-by-side overlapping comparisons, there has been a lack of sufficient analyses of the instrument shelters that house

thermometers. This is potentially a serious matter because thermometers in the nineteenth century were exposed to the open air on north-facing walls when in the twentieth century the thermometers were exposed inside Cotton Region Shelters (CRS) or Stevenson shelters. New automated weather stations in the 1980's (Hubbard et al., 1983) and the new federal Automated Surface Observing System (ASOS) network of the 1990's both introduced thermometer shelters of yet another design.

Temperature equipment at a weather station consists of a thermometer(s) for sensing **air** temperature and a sensor shelter referred to as the radiation shield. The primary function of the radiation shield is to shield the thermometer(s) from direct radiation that would otherwise raise the thermometer temperature much above the **air** temperature. The radiation shield usually is constructed with louvers--ventilating slits that allow air to circulate past the thermometers. Throughout the history of weather station networks changes in instrumentation have occurred; usually a change in the radiation shield design accompanied a change in sensors. Changes in equipment could potentially result in local biases in the temperature record because radiation shields of different design may not have the same ability to **screen out radiation** and to **ventilate the temperature sensor(s)**.

There have been a number of previous studies investigating the characteristics of both air temperature radiation shields and air temperature sensors, including field and wind tunnel tests to determine the errors of air temperature measurement by MacHattie (1965) and Fuchs and Tanner (1965). McKay and McTaggart-Cowan (1977) suggested that air temperature errors caused by radiation shield changes ranged from -0.5 to 1.0°C. McTaggart-Cowan and McKay (1976) performed field comparisons of 14 different shields. They found that using

unaspirated shields without knowledge of other parameters (e.g., radiation and wind) can make relative accuracies uncertain by as much as 1.0°C, and the worst case was a shield that had errors of 2.5°C in light wind conditions. Gill (1983) conducted wind tunnel tests of several radiation shields under high radiation and low wind speed conditions. He found that the Gill shield, a multi-plate plastic shield which currently is in wide service in the automated weather station networks, can introduce +5.2 to 7°C radiation heating errors when the simulated solar intensity is 1080 W m⁻² at a 0.25 m s⁻¹ ambient wind speed. Even with high radiation errors, the Gill was found to be the best of several radiation shields in his experiments. Brock et al. (1995a, 1995b) and Richardson and Brock (1995) explored optimal radiation shield designs and sensor geometry designs with a goal of minimizing both direct and indirect radiation loadings while maximizing the air flow.

In recent years, the National Weather Service (NWS) has gradually replaced the traditional Liquid-in-Glass (LIG) self-registering maximum-minimum thermometers mounted in the CRS with thermistors mounted in plastic multi-plate shields which are called the Maximum-Minimum Temperature System (MMTS). Based on thousands of comparisons of monthly mean temperatures from stations with and without MMTS, Quayle et al. (1991) found that the MMTS temperature system produced maximum temperatures about 0.3°C lower and minimum temperatures about 0.4°C higher than the CRS system. Tanner (1990) stated that it is possible that the Gill shield could produce errors in excess of 5°C over snow covered surfaces with no wind. McKee et al. (1995) reported that systematic temperature differences between ASOS and conventional observations reached -1.2°C for daily maximum and -1.1°C for daily minimum temperatures.

In view of the preceding, it appears each **air** temperature monitoring system creates its own microclimate because of two non-independent factors: **shielding of sensors from radiation** and **ventilation of air** by natural or forced air movement. In this study we monitor the microclimate inside thermometer shelters and describe the microclimate inside the shield as a function of wind condition, solar, and infrared radiation. The overall goal of this study is to investigate the effects of temperature measurement systems (the thermometer and radiation shield) on the normal operating air temperature and to develop a physical model capable of removing such effects. The procedures will include both direct experimentation with an array of temperature equipment that represents major types of temperature systems (CRS, Gill, MMTS, and ASOS) (Figure 1.1) used historically or presently in weather station networks and modeling to increase our physical understanding of air temperature measurement in weather station networks. The specific objectives are to:

1. Theoretically investigate air temperature errors inside radiation shields.
2. Experimentally determine the air flow characteristics inside the shields.
3. Develop a physical model to understand the microclimate inside the shields including the interior solar radiation, infrared radiation, and air flow effects on the air (sensor) temperature under day and night conditions.
4. Experimentally estimate the effect of underlying ground surface coverings on the shield's interior solar radiation.

Each Chapter deals with one objective beginning with Chapter 2.

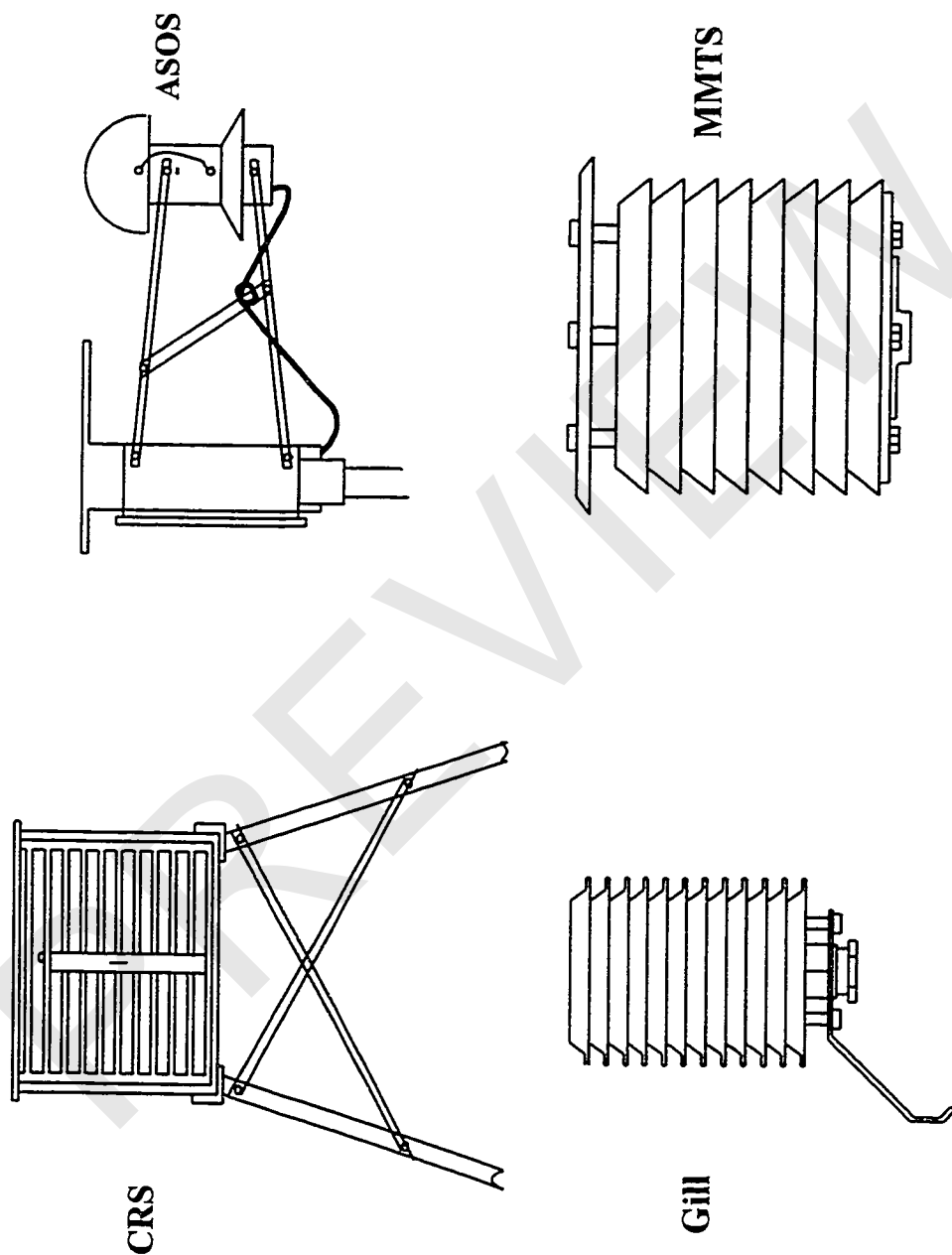


Figure 1.1 Air temperature radiation shields: the standard NWS Cotton Region Shield (CRS); Gill; the Maximum-Minimum Temperature System (MMTS); and the Hygrothermometer of the Automated Surface Observing System (ASOS).

CHAPTER 2

INVESTIGATION OF RADIATIVE ERROR INSIDE AIR TEMPERATURE RADIATION SHIELDS

2.1 INTRODUCTION

2.1.1 Background

An air temperature observation system in a weather station network commonly contains an air temperature sensor and an air temperature radiation shield. The purpose of the air temperature radiation shield is to house the air temperature sensors and in so doing prevent the sun's direct rays from reaching the sensor surface while allowing adequate ventilation and serve as shelter from inclement weather. Advances in semiconductor technology have led to air temperature sensors with accuracies of $\pm 0.1^{\circ}\text{C}$ in controlled conditions. However, in practice, it has been impossible to achieve this accuracy because air temperature radiation shields do not completely shield solar radiation without retarding natural air flow. Adequate air flow is required in order for the sensors to reach thermal equilibrium with the air. Forced ventilation ensures adequate flow but, requires too much power for remote stations. The greatest source of air temperature measurement error is inadequate coupling with the atmosphere (Brock et al., 1995).

The Cotton Region shield (CRS) was used in the U.S. for several decades as the principal air temperature shield. This large wooden structure provides enough space to house